Observation of magnetic adatom-induced Majorana vortex and its fusion with field-induced Majorana vortex in an iron-based superconductor

Peng Fan
Institute of Physics, Chinese Academy of Sciences
Fazhi Yang
Beijing National Laboratory for Condensed Matter Physics and Institute of Physics, Chinese Academy of Sciences
Guojian Qian
Institute of Physics, Chinese academy of sciences
Hui Chen
Institute of Physics, Chinese Academy of Sciences https://orcid.org/0000-0002-3369-8113
Yu-Yang Zhang
University of Chinese Academy of Sciences, Chinese Academy of Sciences https://orcid.org/0000-0002-9548-0021
Geng Li
Institute of Physics & University of Chinese Academy of Sciences, Chinese Academy of Sciences https://orcid.org/0000-0002-3347-7222
Zihao Huang
Institute of Physics, Chinese Academy of Sciences
Yuqing Xing
Institute of Physics, Chinese academy of sciences https://orcid.org/0000-0002-8646-6631
Lingyuan Kong
Institute of Physics, Chinese Academy of Sciences https://orcid.org/0000-0002-0012-8341
Wenyao Liu
Beijing National Laboratory for Condensed Matter Physics and Institute of Physics, Chinese Academy of Sciences
Kun Jiang
Boston College
Chengmin Shen
Institute of Physics, Chinese Academy of Sciences
Shixuan Du
John Schneeloch
Brookhaven National Laboratory

Ruidan Zhong
Brookhaven National Laboratory
Genda Gu
Brookhaven National Laboratory
Ziqiang Wang
Boston College
Hong Ding
Beijing National Laboratory for Condensed Matter Physics and Institute of Physics, Chinese Academy of Sciences https://orcid.org/0000-0003-4422-9248
Hong-Jun Gao (**hjgao@iphy.ac.cn**)
Institute of Physics https://orcid.org/0000-0001-9323-1307

Article

Keywords: magnetic adatom-induced Majorana vortex, field-induced Majorana vortex, fault-tolerant topological quantum computing, braiding

Posted Date: September 21st, 2020

DOI: https://doi.org/10.21203/rs.3.rs-72679/v1

Version of Record: A version of this preprint was published at Nature Communications on March 1st, 2021. See the published version at https://doi.org/10.1038/s41467-021-21646-x.

Abstract

Braiding Majorana zero modes is essential for fault-tolerant topological quantum computing. Iron-based superconductors with nontrivial band topology have recently emerged as a surprisingly promising platform for creating distinct Majorana zero modes in magnetic vortices in a single material and at relatively high temperatures. The magnetic field-induced Abrikosov vortex lattice makes it difficult to braid a set of Majorana zero modes or to study the fusion of a Majorana doublet due to overlapping wave functions. Here we report the observation of the proposed quantum anomalous vortex with integer quantized vortex core states and Majorana zero mode induced by magnetic Fe adatoms deposited on the surface and the realization of its fusion with a nearby field-induced Majorana vortex in iron-based superconductor $FeTe_{0.55}Se_{0.45}$. We also observe vortex-free Yu-Shiba-Rusinov bound states at the Fe adatoms with a weaker coupling to the substrate, and discover a reversible transition between Yu-Shiba-Rusinov states and Majorana zero mode by manipulating the exchange coupling strength. The dual origin of the Majorana zero modes, from magnetic adatoms and external magnetic field, provides a new single-material platform for studying their interactions and braiding in superconductors bearing topological band structures.

Background

The band structure of iron-based superconductor $FeTe_{0.55}Se_{0.45}$ has a nontrivial Z_2 topological invariant and supports helical Dirac fermion topological surface states (TSS)[1, 2], which was confirmed recently by spin-resolved and angle-resolved photoemission spectroscopy[3]. Remarkably, below the bulk transition temperature T_c, superconducting (SC) TSS were observed with a pairing gap[3]. This makes $FeTe_{0.55}Se_{0.45}$ a novel single-material platform for generating Majorana zero modes (MZMs) at the ends of a vortex line[2, 4, 5]. Recently, strong evidence of MZMs inside the magnetic field induced vortices have been observed by scanning tunneling microscope/spectroscopy (STM/S) on the vortex lattice of this type-II superconductor[6-9].

This Majorana platform also presents new challenges for the basic understanding of defect excitations in superconductors with a topological nontrivial band structure, and new possibilities for creating MZMs under different physical conditions. In general, superconductors can host two kinds of defect excitations as in-gap bound states: the Yu-Shiba-Rusinov (YSR) states[10-17] localized at a magnetic impurity and the Caroli-de-Gennes-Matricon (CdGM) states[18-26] inside a magnetic vortex core. To date, these excitations have appeared distinctly in nature; a magnetic impurity induces the YSR states carrying spin, whereas an external magnetic field creates vortices of the whirling supercurrents. In stark contrast to the traditional YSR states, robust zero-bias peaks (ZBPs), sharing the quintessential spectroscopic properties of MZMs, were observed by STM/S at the magnetic interstitial Fe impurities in $FeTe_{0.55}Se_{0.45}$[27], but without applying a magnetic field. A recent theoretical proposal[28] attributes the observed ZBP to a MZM bound to a quantum anomalous vortex (QAV) nucleated spontaneously at the magnetic Fe atom. The role of the magnetic field is played by the exchange coupling of the spin and orbital moment of the Fe impurity

located at the C_4 symmetric sites, which generates circulating supercurrents by the spin-orbit coupling and modulates the phase of the superconducting order parameter. When the exchange coupling is strong enough, a condition favored by the very small Fermi energy (~ 5meV) in $FeTe_{0.55}Se_{0.45}$[3], a transition from the vortex-free YSR states to the QAV was predicted to take place[28]. A MZM emerges inside the QAV core from the superconducting TSS, since the Berry phase of the Dirac fermions transforms the total angular momentum quantum number of the CdGM vortex core states[18] into integers, naturally supporting a zero-energy bound state[8, 28].

Results

To probe the remarkable nature of defect excitations in the superconducting TSS, we deposit magnetic Fe adatoms on the cleaved (001) surface of a single crystal of $FeTe_{0.55}Se_{0.45}$ (Fig. 1a-b) with the substrate temperature below 20 K. Before depositing the Fe adatoms, we scan the surface to ensure that there is no interstitial Fe adatom (See Supplementary Note I), to avoid the mix of interstitial Fe adatoms and deposited Fe adatoms. In contrast to the growth-induced interstitial Fe impurity in the bulk, the adsorbed Fe adatoms are distributed at varies heights above the surface and in different planar locations with respect to the C_4 symmetry sites. As a result, the magnetic Fe adatoms with varying exchange couplings reveal much richer phenomena of the defect excitations of the superconducting TSS.

The STM image of a surface region after the atomic deposition (Fig. 1c) shows scattered Fe adatoms as the bright spots with a coverage of ~0.04 %. The zero-energy dI/dV map in the same area of Fig. 1c, displays relatively high density of states at the locations of the Fe adatoms (Fig. 1d), consistent with the physical picture that magnetic Fe impurities generate in-gap states. From the statistics of more than one hundred measurements (Supplementary Note I, Fig. S2), we identify two types of in-gap states localized around the Fe adatoms with distinct dI/dV spectra exemplified in Fig. 1e. The type-I adatoms, which represent about 10% of our measurements, exhibit a sharp ZBP reminiscent of a MZM coexisting with other in-gap states in the dI/dV spectrum. In contrast, the conductance spectrum of the type-II adatoms, which represent about 90% of our measurements, shows the YSR states, featuring a pair of in-gap states at particle-hole symmetric peak energy positions, but with asymmetric peak weights. In comparison, the typical dI/dV spectrum on the clean surface without the adatom shows a hard superconducting gap without in-gap states (Fig. 1e).

We begin with the type-I Fe adatoms. A high-resolution topographic image (Fig. 2a) shows an isolated type-I adatom. A circular pattern appears in the zero-energy dI/dV map in the vicinity of the Fe site (Fig. 2b), with the zero-energy intensity center slightly offset from the Fe site. The waterfall-like dI/dV spectra (Fig. 2c) and the intensity plot (Fig. 2d) along the red dashed line-cut in Fig. 2a clearly resolve the ZBP and other peaks at nonzero energies inside the superconducting gap. The ZBP persists to about 2.5 nm from the center, indicating the existence of a localized zero-energy state bound to the Fe adatom with the spatial extent comparable to that of the MZM in a magnetic field-induced vortex core in $FeTe_{0.55}Se_{0.45}$[6]. To explore the nature of the discretized in-gap states, we extract several dI/dV spectra from Fig. 2c and

show them as a stacking plot in Fig. 2e. Doing so accounts for the spatial distributions of the in-gap states and the sample inhomogeneity[6, 7] due to Te/Se alloying, which has proven to be useful for studying the core states of magnetic field-induced vortices in $FeTe_{0.55}Se_{0.45}$[8]. The sequence of discretized bound states, including the zero-energy state, is clearly visible as the pronounced peaks labeled by L_0, $L_{\pm1}$, $L_{\pm2}$. The energy positions of the conductance peaks (L_n) are plotted in Fig. 2f. Intriguingly, the average energies (solid lines) of the discrete quantum states bound to the Fe adatom follow closely a sequence of integer quantization , with the minigap meV, the same integer sequence (with a minigap ~ 0.6 meV) followed by the quantized vortex core states observed recently[8] in magnetic field-induced vortices that host the MZM[6, 7]. The different values of the minigap are caused by the fluctuation of the superconducting gap Δ and Fermi energy E_f on different surface, due to the inhomogeneous Te and Se atoms in $FeTe_{0.55}Se_{0.45}$. More cases are shown in Supplementary Fig. S3 for the type-I Fe adatoms. Such an integer quantized sequence is the hallmark of the CdGM vortex core states of the superconducting TSS in the quantum limit[8, 28]. Our observations thus provide substantiated and compelling evidence that vortex-like topological defect excitations such as the QAVs nucleate spontaneously at the type-I Fe adatoms and the ZBP corresponds to a vortex MZM.

It is necessary to check the temperature and magnetic field dependence of the ZBP, since a vortex MZM would respond differently than vortex-free defect states. The temperature evolution of the ZBP on the Fe adatom turns out to be very similar to that of the MZM in a field-induced vortex[6]. The ZBP intensity of the center spectrum pointed by the black arrow in Fig. 2c decreases with increasing temperatures, and becomes almost invisible at 4.2 K (Fig. 2g). The magnetic field dependence is also very similar to that of a vortex MZM as the ZBP does not split or broaden for fields up to 8 T (Fig. 2h), provided that no field-induced vortices enter the region near the adatom when the magnetic field is applied. The ZBP is however sensitive to the location of the adsorbed Fe adatom. We found that all type-I adatoms producing integer quantized bound states anchored by the ZBP are adsorbed at the high-symmetry sites in the center of four Te/Se atoms. To test the robustness of this finding, we manipulate a type-I adatom by the STM tip to a different location away from the C_4 symmetric site. The ZBP disappears and a pair of in-gap state at nonzero energy emerges (Supplementary Note III and Fig. S4). After annealing the sample to 15 K and perform the measurement again at 0.4 K, the adatom diffuses back to its original high-symmetry site and the ZBP reappears. Thus, the high-symmetry site is a prerequisite for the induced ZBP, which agrees with the proposed theory that the orbital magnetic moment of the Fe adatoms at C_4 symmetric locations plays an important role for the nucleation of the QAV[28].

Next, we turn to study the type-II Fe adatoms (Supplementary Note IV). In contrast to the type-I adatoms, the conductance exhibits predominantly a pair of in-gap peaks at nonzero energies without the ZBP. Applying an external magnetic field, we observe that the peaks shift approximately linearly to higher energies (Supplementary Fig. S5d) away from the Fermi level, consistent with a pair of spin-polarized YSR in-gap states. We find that the type-II Fe adatoms are adsorbed at myriad locations on or off the high-symmetry axis and induce YSR states at different energies, indicative of broadly varying exchange

couplings to the superconducting quasiparticles. In special cases, we also observe YSR states located very close to zero energy, which nevertheless split under the magnetic field (Supplementary Note IV and Fig. S6) and are therefore distinct from the robust ZBP observed on the type-I Fe adatoms.

These observations motivate us to manipulate the exchange coupling between the magnetic adatoms and the substrate by tuning the tip to sample distance[29, 30]. The electrostatic force of an approaching tip can prod and move the Fe adatom in directions parallel and perpendicular to the surface (Fig. 3a), which can affect the atomic orbital moment of the Fe adatom and the spin-orbit exchange coupling to the superconductor. In STM/S, the tunnel-barrier conductance G_N , where I_t is the tunneling current and V_s is the bias voltage, governs the tunnel coupling and changes with the tip-sample distance. Performing tunneling conductance measurements as a function of G_N, we find that the energies of the YSR states are modulated ubiquitously when the tip approaches the type-II Fe adatoms (Supplementary Note V). The observed crossing and reversal of the in-gap states (Supplementary Fig. S7), a trademark of the YSR states, confirms that reducing the tip to sample distance monotonically increases the exchange coupling between the Fe atom and the superconductor.

Unexpectedly, as the STM tip approaches a significant number of the type-II Fe adatoms (~ 27%), the pair of YSR states modulates with increasing G_N, but then coalesces in a captivating manner into a single ZBP in the water-fall plot of dI/dV spectra (Fig. 3c) and the intensity plot (Fig. 3d), which remains robust under further increase of the barrier conductance. Note that the emergence of the ZBP out of the YSR states is different from the transition point between the screened spin-singlet and doublet ground states[29, 31], where the two YSR states are approximately degenerate at zero energy as marked by the red arrow in Fig. 3d. To probe the change in the nature of the in-gap states with different barrier conductance, we repeated the entire process under an applied magnetic field. The dI/dV spectra and the intensity plot obtained under 6 T (Fig. 3e-f) show that the vortex-free YSR states no longer cross zero energy, due to the Zeeman splitting that removes the accidental degeneracy. However, the emergence of the unsplit ZBP at higher G_N is unabridged even at such a high field, indicating that ZBP corresponds to a single MZM robust against an applied magnetic field. This identification is further corroborated by performing the measurements on type-I Fe adatoms that show the ZBP associated with the MZM upholds its integrity and does not shift or split with increasing G_N in a field as high as 6 T (Supplementary Note VI and Fig. S8). The compelling evidence attributes the novel coalescence of in-gaps states to the ZBP as a topological transition (Fig. 3b) from the vortex-free YSR states to a vortex MZM, which is fully consistent with the theoretical prediction that increasing the exchange coupling of an Fe impurity induces a transition from the YSR states to the QAV states hosting a MZM in $FeTe_{0.55}Se_{0.45}$ superconductors[28]. The transition between the YSR states and the MZM is even reversible, as the dI/dV spectra as a function of the barrier conductance retrace that shown in Fig. 3e-f upon withdrawing the tip (Fig. 3g-h) in a controlled manner. The transition is also replicable when the type-II Fe adatom under the tip in Fig. 3 is moved to a different location about 1 nm away (Supplementary Fig. S9). These observations reveal the unprecedented nature of defect excitations in the superconducting TSS where local magnetic moment and screening currents are inextricably connected through the magnetoelectric effect.

The phase coherence of the MZMs is stored nonlocally and protected by the topological degeneracy against the ravages of environmental decoherence caused by local perturbations, which is the central to the idea of topological quantum computing[32, 33]. The coupling of two MZMs sufficiently close by annihilates of the nonabelian anyonic zero modes and creates a pair of fermionic states at nonzero energies. This fusion process usually requires two overlapping magnetic field induced vortices, which is difficult to control on the Abrikosov lattice[7, 8, 34]. Our system allows a new possibility, i.e., the fusion between MZMs hosted in a QAV and a field-induced vortex (Fig. 4). The zero-energy dI/dV map (Fig. 4a) shows a MZM in the QAV nucleated at a type-I Fe adatom in a magnetic field of -0.2 T, also visible in the intensity plot (Fig. 4b) as sharp ZBPs along the line cut across the adatom. A field-induced vortex is observed to enter the field of view subsequently. The latter sits very close to the Fe site, thus enlarges significantly the region with spectral weight at zero-energy (Fig. 4c). Remarkably, acquiring the intensity plot along the same line cut shows that the ZBP splits into two peaks separated by an energy spacing ~ 0.25 meV (Fig. 4d). During the second round of the measurements, the vortex creeps away. The zero-energy map recovers (Fig. 4e) and the ZBP reemerges in the intensity plot (Fig. 4f). Throughout the fusion process, the temperature and the magnetic field are kept stable. It is necessary to point out that the creeping of the vortices is observed quite often when we detected MZMs in the filed-induced vortices in our previous work. Three representative dI/dV spectra corresponding to the three conditions are extracted and displayed in Fig. 4g for a better comparison. Repeating the measurements on the same Fe adatom in a higher magnetic field of -3 T reveals again the splitting of the ZBP caused by the presence of a nearby field-induced vortex (Fig. 4h), with a larger energy spacing ~ 0.35 meV (Fig. 4i), possible due to the shorter distance and stronger overlap of the two MZMs as indicated by the smaller ring feature in the zero-energy map in Fig. 4h compared to Fig. 4c. Moreover, a field-induced vortex can also enter the field of view without causing detectable splitting of the ZBP bound to the Fe adatom or the vortex MZM when they are relatively far apart (Supplementary Note VIII and Fig. S10). These observations further support the identification of the ZBP induced by type-I Fe atoms as the MZM and concurrently provide the first experimental evidence for the fusion between two vortex MZMs as illustrated in Fig. 4j.

Discussion

Our STM/S measurements on magnetic Fe adatoms deposited on the surface of $FeTe_{0.55}Se_{0.45}$ superconductors revealed the spontaneous formation of anomalous vortex matter with integer quantized core states and MZMs in zero external field, and the reversible transition between a YSR impurity and a QAV with increasing exchange interaction strength. These fundamental properties, previously unobserved in superconductors, are consistent with the predications of the theoretical proposal of the QAV[28]. They have broad implications for superconductors with a nontrivial topological band structure and spin-momentum locked superconducting TSS, which have also been found in several other iron-based superconductors such as LiFeAs[35, 36], $(Li_{0.84}Fe_{0.16})$OHFeSe[37], and $CaKFe_4As_4$[38]. Together with the observed fusion of the MZMs in the QAV nucleated at the Fe adatom and the nearby field-induced Abrikosov vortex, our findings demonstrate that magnetic adatoms coupled to the superconducting TSS

provide a realistic materials platform for creating and studying the interactions between the nonabelian topological vortex MZMs.

Methods

High-quality single crystals of $FeTe_{0.55}Se_{0.45}$ with Tc of 14.5K are grown using the self-flux method[6]. The samples are cleaved in situ and immediately transferred into a STM head. The Fe adatoms are deposited from a high-purity (99.95%) single crystal Fe rod acquired from *ESPI METALS* to the surface of $FeTe_{0.55}Se_{0.45}$ at a temperature below 20 K. Before Fe deposition, we scan the surface of $FeTe_{0.55}Se_{0.45}$ to ensure that there were no visible interstitial Fe impurities (IFI). The STM experiments are performed in an ultrahigh vacuum (1×10^{-11} mbar) LT-STM systems (USM-1300s-^{3}He), which can apply a perpendicular magnetic field up to 11 T. STM images are acquired in the constant-current mode with a tungsten tip. The energy resolution calibrated on a clean Pb (111) surface is about 0.27 meV. The voltage offset calibration is followed by a standard method of overlapping points of I-V curves. Differential conductance (dI/dV) spectra are acquired by a standard lock-in amplifier at a frequency of 973.1 Hz, under modulation voltage V_{mod} = 0.1 mV. Low temperature of 0.4 K is achieved by a single-shot ^{3}He cryostat.

Data availability

All relevant data are available from the corresponding authors upon reasonable request.

Declarations

Acknowledgements

We thank Xi Dai, Shengshan Qin, Shiyu Peng, Sankar Das Sarma for useful discussions. The work at IOP is supported by grants from the National Natural Science Foundation of China (11888101, 61888102 and 11674371), the National Key Research and Development Projects of China (2016YFA0202300, 2018YFA0305800 and 2019YFA0308500), and the Chinese Academy of Sciences (XDB28000000, XDB07000000, 112111KYSB20160061). The work at BNL and BC is supported by grants from US DOE, Basic Energy Sciences (DE-SC0012704, DE-FG02-99ER45747).

Author contributions

H.-J. G. and H.D. designed STM experiments. P.F., G.Q. and H.C. performed STM experiments with assistance of F.Y., Z.H. and Y.X.. J.S., R.Z. and G.G. provided samples. K.J. and Z.Q.W. provided theoretical explanations. P.F., F.Y., G.Q. and H.C. processed experimental data and wrote the manuscript with input from all other authors. All the authors participated in analyzing experimental data, plotting figures, and writing the manuscript. Z.Q.W., H.D. and H.-J. G. supervised the project.

Competing interests:

The authors declare that they have no competing interests.

References

1. Wang, Z. J. et al. Topological nature of the $FeSe_{0.5}Te_{0.5}$ superconductor. *Phys Rev B* **92**, 115119 (2015).
2. Xu, G., Lian, B., Tang, P. Z., Qi, X. L. & Zhang, S. C. Topological superconductivity on the surface of Fe-based superconductors. *Phys Rev Lett* **117**, 047001 (2016).
3. Zhang, P. et al. Observation of topological superconductivity on the surface of an iron-based superconductor. *Science* **360**, 182-186 (2018).
4. Hosur, P., Ghaemi, P., Mong, R. S. & Vishwanath, A. Majorana modes at the ends of superconductor vortices in doped topological insulators. *Phys Rev Lett* **107**, 097001 (2011).
5. Fu, L. & Kane, C. L. Superconducting proximity effect and majorana fermions at the surface of a topological insulator. *Phys Rev Lett* **100**, 096407 (2008).
6. Wang, D. F. et al. Evidence for Majorana bound states in an iron-based superconductor. *Science* **362**, 333-335 (2018).
7. Machida, T. et al. Zero-energy vortex bound state in the superconducting topological surface state of Fe(Se,Te). *Nat Mater* **18**, 811-815 (2019).
8. Kong, L. et al. Half-integer level shift of vortex bound states in an iron-based superconductor. *Nat Phys* **15**, 1181-1187 (2019).
9. Zhu, S. Y. et al. Nearly quantized conductance plateau of vortex zero mode in an iron-based superconductor. *Science* **367**, 189-192 (2020).
10. Yu, L. Bound state in superconductors with paramagnetic impurities. *Acta Phys Sin* **21**, 75-91 (1965).
11. Shiba, H. Classical spins in superconductors. *Prog Theor Phys* **40**, 435-451 (1968).
12. Rusinov, A. I. & Fiz., P. M. Z. E. T. On the theory of gapless superconductivity in alloys containing paramagnetic impurities. *JETP Lett* **9**, 1101-1106 (1968).
13. Yazdani, A., Jones, B. A., Lutz, C. P., Crommie, M. F. & Eigler, D. M. Probing the local effects of magnetic impurities on superconductivity. *Science* **275**, 1767-1770 (1997).
14. Choi, D. J. et al. Influence of magnetic ordering between Cr adatoms on the Yu-Shiba-Rusinov states of the beta-Bi_2Pd superconductor. *Phys Rev Lett* **120**, 167001 (2018).
15. Cornils, L. et al. Spin-resolved spectroscopy of the Yu-Shiba-Rusinov states of individual atoms. *Phys Rev Lett* **119**, 197002 (2017).
16. Salkola, M. I., Balatsky, A. V. & Schrieffer, J. R. Spectral properties of quasiparticle excitations induced by magnetic moments in superconductors. *Phys Rev B* **55**, 12648-12661 (1997).
17. Flatté, M. E. & Jeff M. Byers. Local electronic structure of a single magnetic impurity in a superconductor. *Phys Rev Lett* **78**, 3761-3764 (1997).

18. Caroli, C. d. G., P.G. Matricon, J. Bound Fermion states on a vortex line in a type II superconductor. *Phys Lett* **9**, 307-309 (1964).
19. Bardeen, J., Kümmel, R., Jacobs, A. E. & Tewordt, L. Structure of vortex lines in pure superconductors. *Phys Rev* **187**, 556-569 (1969).
20. Hess, H. F., Robinson, R. B. & Waszczak, J. V. Vortex-core structure observed with a scanning tunneling microscope. *Phys Rev Lett* **64**, 2711-2714 (1990).
21. Gygi, F. & Schluter, M. Self-consistent electronic structure of a vortex line in a type-II superconductor. *Phys Rev B* **43**, 7609-7621 (1991).
22. Hayashi, N., Isoshima, T., Ichioka, M. & Machida, K. Low-lying quasiparticle excitations around a vortex core in quantum limit. *Phys Rev Lett* **80**, 2921 (1998).
23. Shan, L. et al. Observation of ordered vortices with Andreev bound states in $Ba_{0.6}K_{0.4}Fe_2As_2$. *Nat Phys* **7**, 325-331 (2011).
24. Hanaguri, T., Kitagawa, K., Matsubayashi, K., Mazaki, Y., Uwatoko, Y. & Takagi, H. Scanning tunneling microscopy/spectroscopy of vortices in LiFeAs. *Phys Rev B* **85**, 214505 (2012).
25. Massee, F. et al. Imaging atomic-scale effects of high-energy ion irradiation on superconductivity and vortex pinning in Fe(Se, Te). *Sci Adv* **1**, e1500033 (2015).
26. Chen, M. et al. Discrete energy levels of Caroli-de Gennes-Matricon states in quantum limit in $FeTe_{0.55}Se_{0.45}$. *Nat Commun* **9**, 970 (2018).
27. Yin, J. X. et al. Observation of a robust zero-energy bound state in iron-based superconductor Fe(Te,Se). *Nat Phys* **11**, 543-546 (2015).
28. Jiang, K., Dai, X. & Wang, Z. Q. Quantum anomalous vortex and Majorana zero mode in iron-based superconductor Fe(Te,Se). *Phys Rev X* **9**, 011033 (2019).
29. Farinacci, L. et al. Tuning the coupling of an individual magnetic impurity to a superconductor: quantum phase transition and transport. *Phys Rev Lett* **121**, 196803 (2018).
30. Malavolti, L. et al. Tunable spin–superconductor coupling of spin 1/2 vanadyl phthalocyanine molecules. *Nano Lett* **18**, 7955-7961 (2018).
31. Hatter, N., Heinrich, B. W., Ruby, M., Pascual, J. I. & Franke, K. J. Magnetic anisotropy in Shiba bound states across a quantum phase transition. *Nat Commun* **6**, 8988 (2015).
32. Kitaev, A. Y. Fault-tolerant quantum computation by anyons. *Ann Phys* **303**, 2-30 (2003).
33. Nayak, C., Simon, S. H., Stern, A., Freedman, M. & Das Sarma, S. Non-Abelian anyons and topological quantum computation. *Rev Mod Phys* **80**, 1083-1159 (2008).
34. Chiu, C. K., Machida, T., Huang, Y. Y., Hanaguri, T. & Zhang, F. C. Scalable Majorana vortex modes in iron-based superconductors. *Sci Adv* **6**, eaay0443 (2020).
35. Zhang, P. et al. Multiple topological states in iron-based superconductors. *Nat Phys* **15**, 41-47 (2019).
36. Zhang, S. S. et al. Field-free platform for Majorana-like zero mode in superconductors with a topological surface state. *Phys Rev B* **101**, 100507 (2020).

37. Liu, Q. et al. Robust and clean Majorana zero mode in the vortex core of high-temperature superconductor ($Li_{0.84}Fe_{0.16}$)OHFeSe. *Phys Rev X* **8**, 041056 (2018).

38. Liu, W. et al. A new Majorana platform in an Fe-As bilayer superconductor. Preprint at https://arxiv.org/abs/1907.00904. (2019).

Figures

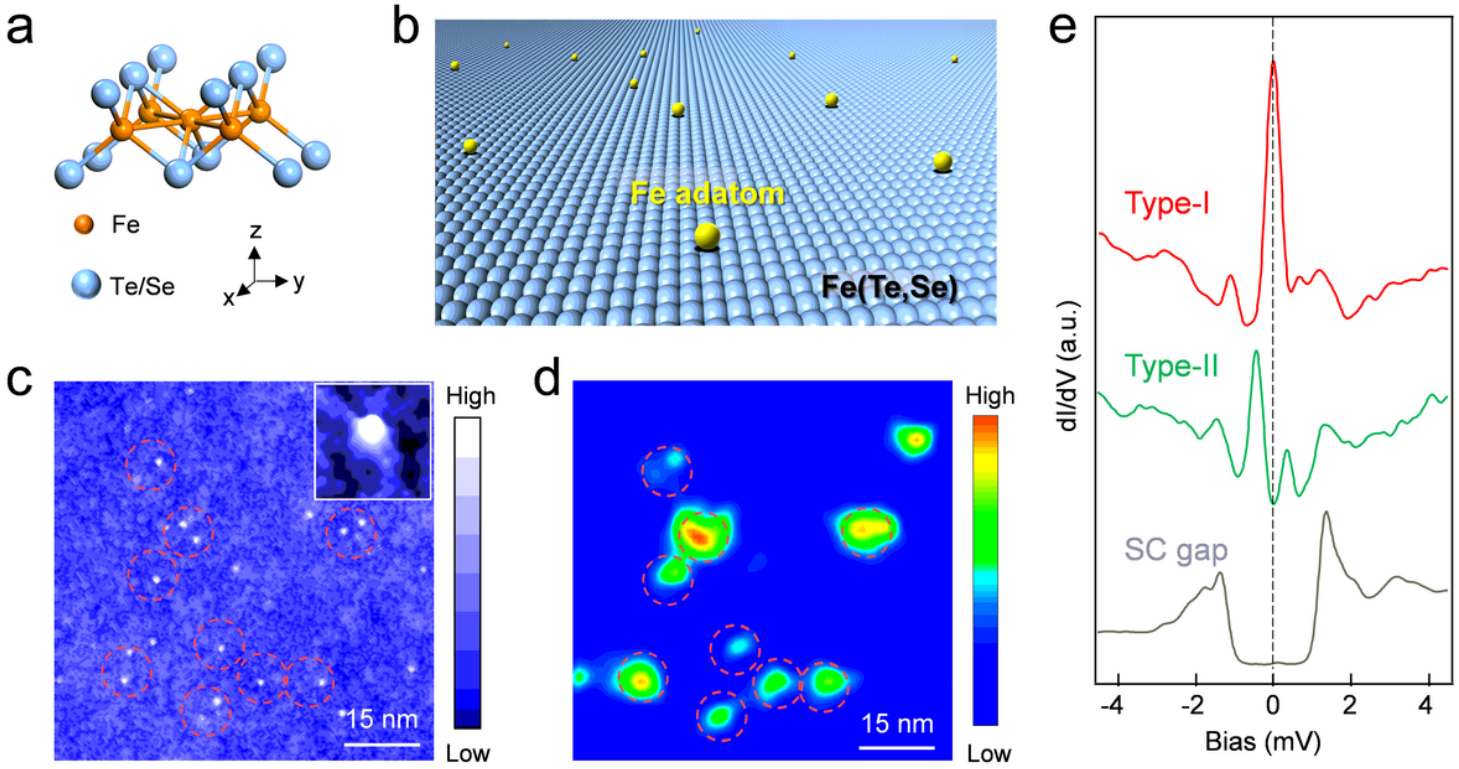

Figure 1

Characterization of deposited Fe adatoms on FeTe0.55Se0.45 surface. a Crystal structure of Fe(Te,Se). b Schematics of Fe adatoms deposited on the surface of FeTe0.55Se0.45. The adsorption sites are random, including both on and off of the C4 symmetric sites in the center of four Te/Se atoms and at various heights above the surface (Supplementary Note I). c A STM image after atomic Fe atom deposition. The bright dots correspond to Fe adatoms with a coverage of 0.04 %. Inset: A 4 nm × 4 nm atomic resolution topographic image showing a single Fe adatom located at a high-symmetry site. d A dI/dV map of c at zero energy. The high conductance areas and the Fe adatom positions are in good spatial correspondence, as highlighted by the red dashed circles. e Typical dI/dV spectra showing the zero bias peak on type-I Fe adatoms (red curve), YSR states (green curve) on type-II Fe adatoms, and the clean superconducting (SC) gap away from the adatoms (gray curve).

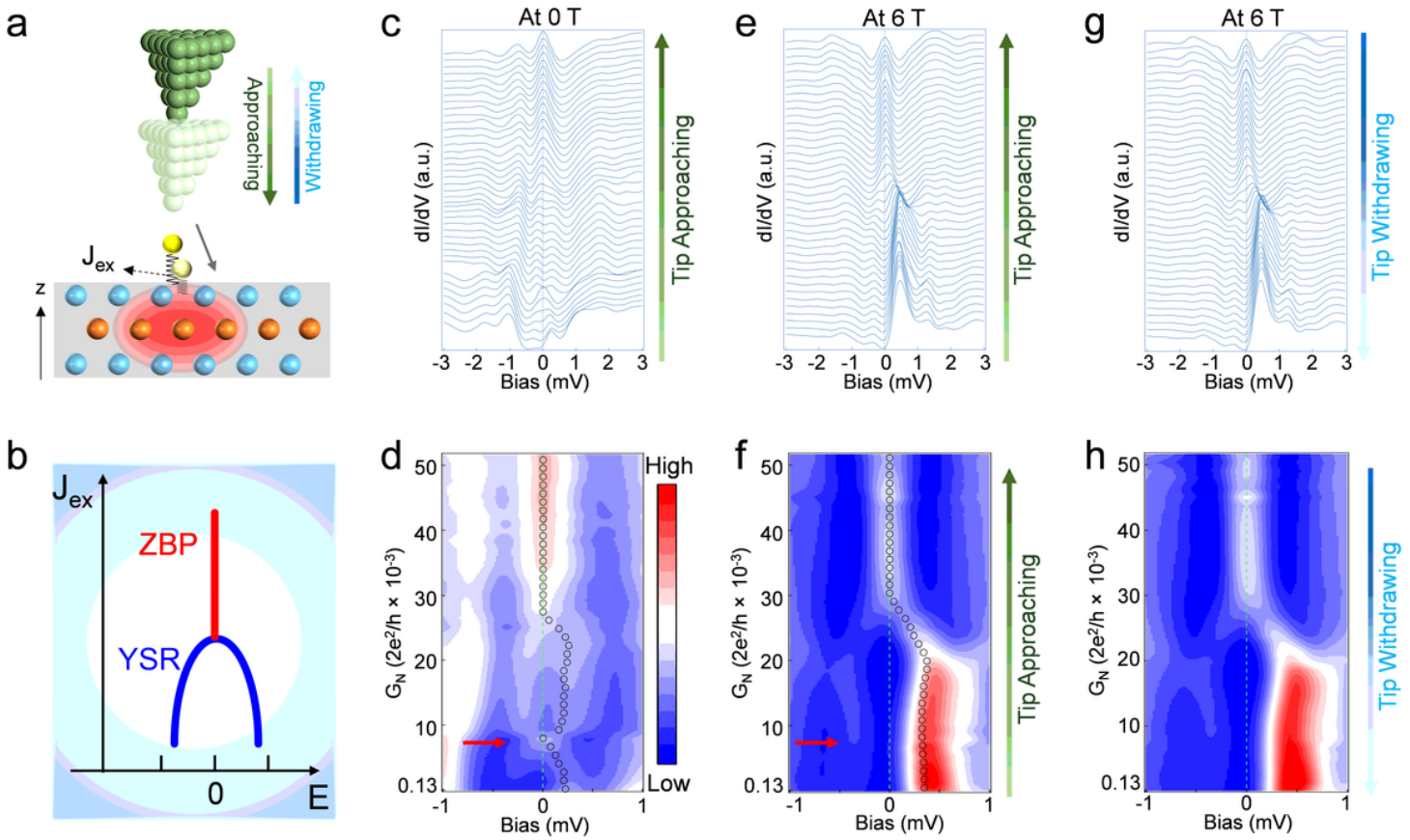

Figure 2

ZBP and integer quantized in-gap states on type-I Fe adatoms. a An atomic-resolution topographic image of a single type-I Fe adatom (red circle). b A zero-energy dI/dV map of the same area in a. c and d dI/dV spectra and the corresponding intensity plot along the line-cut indicated by the red dashed and arrowed line in a and b. The decay length of the ZBP is about 2.5 nm. e A stacking plot of several dI/dV spectra marked by the red arrows in c. The energies of the in-gap states are labeled as L0, L±1, L±2. f The energies of the in-gap states at different spatial positions along the line-cut. Error bars are the FWHM of a Gaussian fit. The energy values of the solid lines are calculated as the average energy of the in-gap states, showing the same integer quantization as the topological vortex core states anchored by the MZM. g Temperature dependence of the dI/dV spectra measured at zero-energy intensity center (white circle in b) with the corresponding spectrum (the black curve) pointed by the black arrow in c. The ZBP intensity decreases with increasing temperature and becomes indiscernible at 4.2 K. h Magnetic field dependence of the dI/dV spectra also acquired at the zero-energy intensity center (white circle in b) at 0.4 K. The ZBP remains robustly at zero energy without splitting.

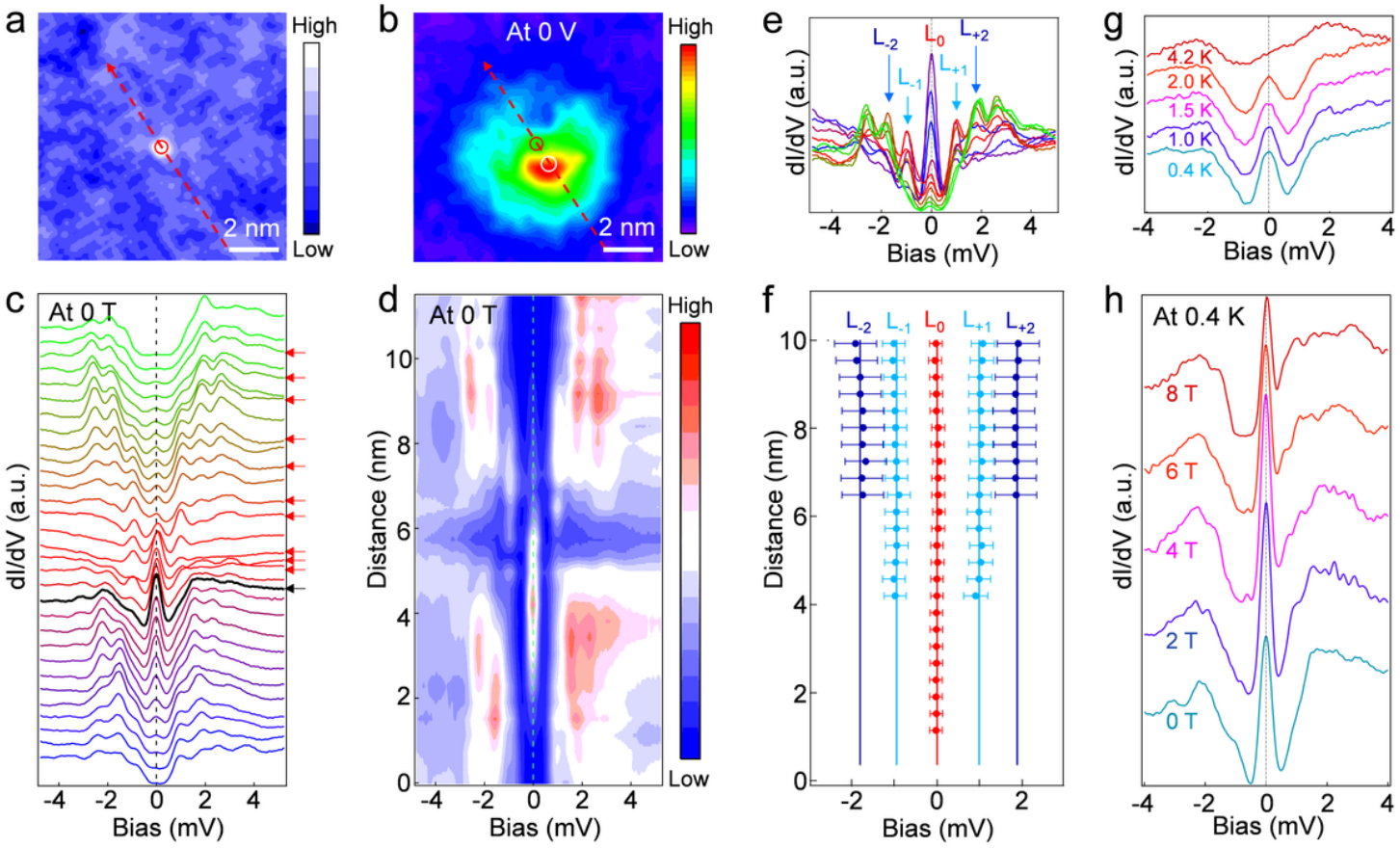

Figure 3

Reversible transitions between YSR states and a robust ZBP/MZM induced by modulating the exchange coupling of type-II Fe adatoms using the STM tip. a Schematics illustrating an approaching STM tip on top of a type-II Fe adatom can move the Fe adatom in directions parallel and perpendicular to the Te/Se surface and modulate the spin-orbit exchange coupling (Jex) to the superconductor. b Schematic phase diagram from the vortex-free YSR states to an anomalous vortex MZM represented by the ZBP with the increasing exchange coupling Jex. c and d Tunnel barrier conductance dependence of the dI/dV spectra in c and its intensity plots in d, showing the evolution of vortex-free YSR states into a robust ZBP at 0 T under an approaching tip. Red arrow in d indicates the position of an accidental near degeneracy of the YSR states. e and f are the same as c and d, but measured in a magnetic field of 6 T. The accidental degeneracy of the YSR states in 0 T in d is removed by the 6T magnetic field, while the evolution to the ZBP remains robust. g and h are the same as e and f, but showing the transition from ZBP to YSR states by withdrawing the STM tip at 6T, indicating the transition is reversible.

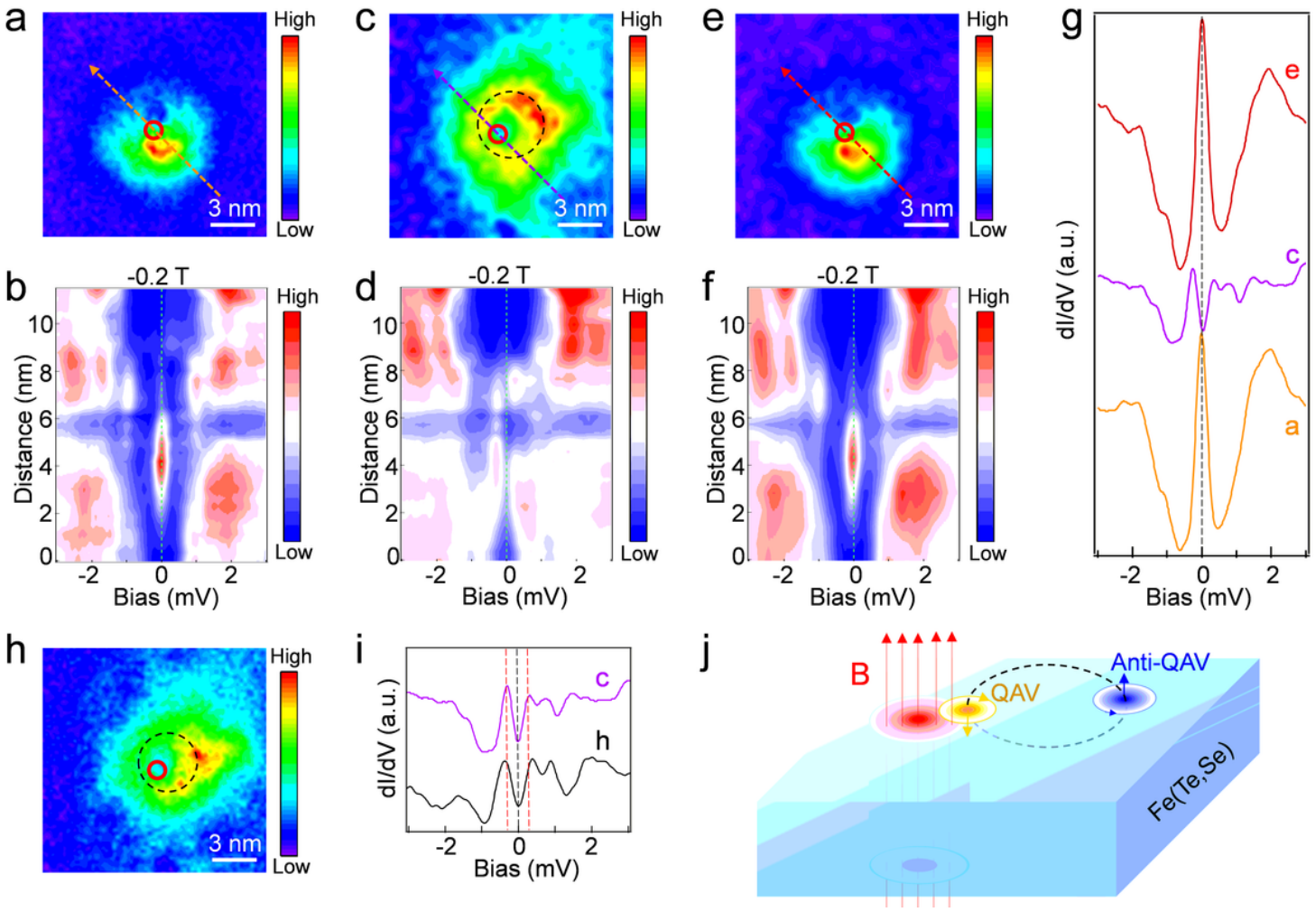

Figure 4

Fusion between two MZMs in the QAV and field-induced vortex. a Zero-energy dI/dV map around a type-I Fe adatom in a magnetic field of -0.2 T, showing the spatial distribution of the MZM in an isolated QAV nucleated at the adatom. b Intensity plot of dI/dV spectra along the line-cut indicated by the arrowed red dashed line in a, showing a robust ZBP. c and d are the same as a and b, but with an additional field-induced vortex pinned near the same Fe adatom visible in the zero-energy map in c. The ZBP disappears in the intensity plot of the dI/dV spectra along the same line-cut in d and two in-gap states with an energy level spacing of 0.25 meV emerge. e and f are the same as c and d, but after the field-induced vortex creeps away. The MZM returns and the zero-energy dI/dV map and the intensity plot of the dI/dV spectra along the line cut recover those in a and b. g Three dI/dV spectra obtained on the Fe adatom in a, c, and e (Vs = -10 mV, It = 200 pA), respectively. h Zero-energy dI/dV map around the same Fe adatom at -3T (Vs = -10 mV, It = 100 pA), showing an additional field-induced vortex pinned close to the adatom. i dI/dV spectra obtained on the Fe adatom in h and c (Vs = -10 mV, It = 200 pA). Both spectra show disappearance of ZBP and emergence of two in-gap states separated by an energy spacing that is larger (0.35 meV) in the case of h compared to c (0.25 meV). j Schematics of the interaction between two MZMs in the QAV and the field-induced vortex.

Supplementary Files

This is a list of supplementary files associated with this preprint. Click to download.

- SIFeimpurity.docx